A pseudo active kinematic constraint for a biological living soft tissue: an effect of the collagen network

Christian Bourdarias, Stéphane Gerbi, Jacques Ohayon

A pseudo active kinematic constraint for a biological living soft tissue: an effect of the collagen network

Christian Bourdarias[*], Stéphane Gerbi[†] and Jacques Ohayon[‡]

Abstract

Recent studies in mammalian hearts show that left ventricular wall thickening is an important mechanism for systolic ejection and that during contraction the cardiac muscle develops significant stresses in the muscular cross-fiber direction. We suggested that the collagen network surrounding the muscular fibers could account for these mechanical behaviors. To test this hypothesis we develop a model for large deformation response of active, incompressible, nonlinear elastic and transversely isotropic living soft tissue (such as cardiac or arteries tissues) in which we include a coupling effect between the connective tissue and the muscular fibers. Then, a three-dimensional finite element formulation including this internal pseudo-active kinematic constraint is derived. Analytical and finite element solutions are in a very good agreement. The numerical results show this wall thickening effect with an order of magnitude compatible with the experimental observations.

Keywords : Constitutive law, Finite element method, Living tissue, Hyperelasticity, Nonlinear partial differential equations, Anisotropic material.

1 Introduction

It is known that the transverse shear along myocardial cleavage planes provides a mechanism for a normal systolic wall thickening [14]. Indirect evidences indicate that the characteristics of the passive extracellular connective tissue in the myocardium is an important determinant of ventricular function ([15], [23], [7]). An appropriate constitutive law for the myocardium should therefore incorporate the most important features of its microstructure. A sound theoretical formulation for material laws of the active myocardium is essential for an accurate mechanical analysis of the stresses in the ventricular wall during the whole cardiac cycle. The wall stress distribution is one of the main factors governing the myocardial energetic [25], the coronary blood flow [3], the cardiac hypertrophy [23], and the fetal heart growth [19]. To date we do not have any reliable technique to evaluate the stress in the cardiac muscle, therefore, mechanical models are useful in cardiology to assess the functional capacities of the human heart. Several numerical models using a finite element (FE) analysis have been performed to simulate the left ventricular performance ([13], [29]). The mechanical behavior of the connective tissue is often assumed isotropic [20]. This last assumption is not in agreement with the experimental results obtained on a sample of active myocardial rabbit tissue. Lin and Yin [15] showed that, during an active equibiaxial stretch test, there are significant stresses developed in the cross-fiber direction (more than 40% of those in the fiber direction) that cannot be attributed to nonparallel muscle fibers (MF).
Therefore, the purposes of this paper are to: (i) suggest a realistic pseudo-active kinematic law coupling the passive connective tissue to the muscle fibers, which may explain the developed tension in the cross-fiber direction observed by Lin and Yin ([15]), (ii) formulate an active three-dimensional material law for a nonlinear hyperelastic and incompressible continuum medium, which takes care of these coupling effects, (iii) derive the related three-dimensional finite element (FE) formulation, and (iv) test the accuracy of the proposed numerical method.

[*]Laboratoire de Mathématiques, Université de Savoie, 73376 Le Bourget du Lac, France, email:Christian Bourdarias @univ-savoie.fr

[†]Laboratoire de Mathématiques, Université de Savoie, 73376 Le Bourget du Lac, France, email:Stephane.Gerbi@univ-savoie.fr

[‡]Université Joseph Fourier, Laboratoire TIMC-IMAG, Grenoble, France and Institut de l'Ingénierie et de l'Information de Santé (IN3S) Faculté de Médecine de Grenoble Btiment Taillefer (Bureau B57) 38706 La Tronche Cedex, France, email: Jacques.Ohayon@imag.fr

2 Microstructure of the cardiac tissue

2.1 Muscle fiber organization

Anatomical observations have shown that the cardiac muscle tissue has a highly specialized architecture [26]. This structure is composed primarily of cardiac muscle cells, or myocytes, that are 80 to 100 μm in length and are roughly cylindrical with cross-sectional dimensions of 10 to 20 μm. These cells are arranged in a more or less parallel weave that we idealize as "muscle fibers" (MF). We shall denote the local direction of this group of cells by the unit vector $\mathbf{f}$ and refer to it also as the local "fiber" direction with the understanding that individual continuous MF do not really exist. Experimental measurements have shown that the MF direction field defines paths on a nested family or toroidal surfaces of revolution in the wall of the heart [26]. These results show a continuously changing orientation $\mathbf{f}$ of the MF through the wall, circumferential near the midwall and progressively more inclined with respect to the equatorial plane when moving toward either the epicardium or the endocardium.

2.2 The cardiac connective tissue organization

Myocytes and coronary blood vessels are embedded in a complex extracellular matrix which consists of collagen and elastin, mainly. Caulfield and Janicki [2] used the scanning electron microscope (SEM) to reveal the basic organization of this connective tissue network. Their studies on the connective tissue of mammalian heart muscle give the description of the extracellular structures and their arrangement relative to cardiac muscle cells. They described the three following classes of connective tissue organization: (i) interconnections between myocytes, (ii) connections between myocytes and capillaries and, (iii) a collagen weave surrounding group of myocytes. When viewed by SEM, groups of myocytes can be seen to be encompassed by a rather prominent meshwork of fibrillard collagen, and short collagen struts attach the myocytes subjacent to this meshwork to it.

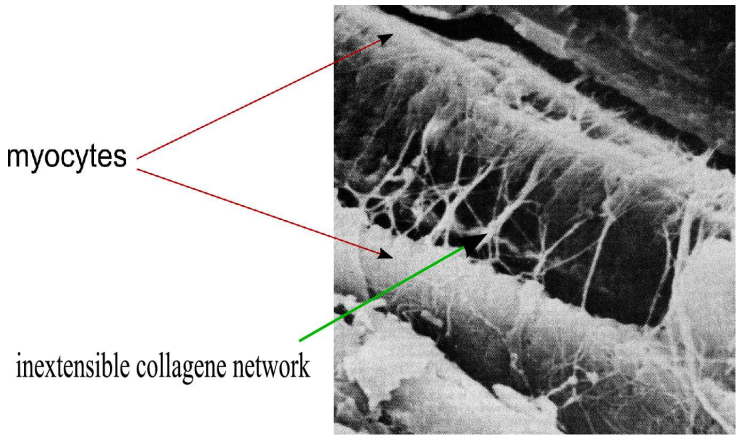

Figure 1: Collagen network surrounding the myocytes.

3 Constitutive law in continuum mechanics

3.1 Coupling between muscle fibers and collagen network

Extrapolations from muscle fiber arrangement to myocardial stress are realistic when also taking account the effect of the connective tissue. We believe that a part of that connective tissue, surrounding group of myocytes, is responsible for active tension developed in the perpendicular direction of the muscle fibers running on the tangential plane of the ventricular wall.
Based on the previous SEM observations, we proposed a connective tissue organization illustrated on Figure 1. We assumed that the myocytes are roughly cylindrical and that groups of myocytes are surrounded by inextensible collagen networks. So, during the contraction, the myocytes diameter increases and because the collagen network is inextensible, the adjacent muscle cells become closer. Thus the pseudo-active kinematic relation between the muscle fiber and cross-fiber extension ratios (noted λ_f and

λ_{cf}, respectively) is $h(\lambda_f, \lambda_{cf}) = 0$ with:

$$h(\lambda_f, \lambda_{cf}) = 1 - \lambda_{cf} + (\pi - 2)(1 - \lambda_f^{-1/2})\frac{a}{D} \tag{1}$$

with $D = 4a + d$ where a is the initial myocyte radius and d is the distance between the two cells.

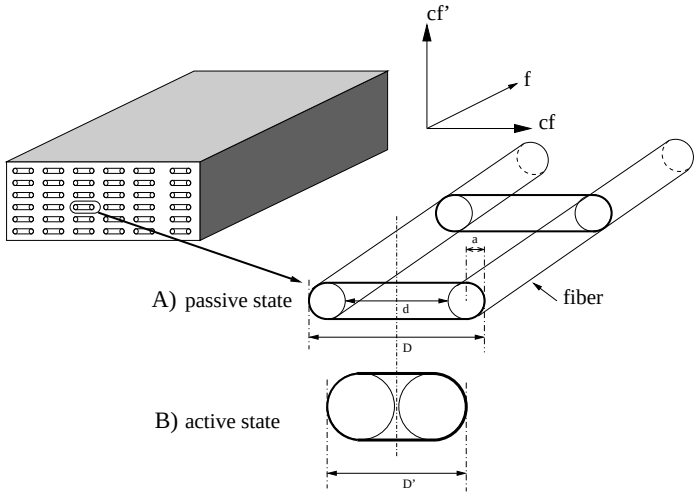

Figure 2: Schematic illustration of the internal pseudo-active kinematic constraint induced by the collagen network surrounding the myocytes. A) Before contraction. B) After or during contraction.

3.2 Constitutive law for the myocardium under internal pseudo-active kinematic constraint

To be consistent with our mathematical formulation, the letter $\mathbf{\Phi}$ is used for non elastic gradient tensor and the letter $\mathbf{F}$ is used for elastic gradient tensor. The activation of the muscle fibers changes the properties of the material and at the same time contracts the muscle itself. To have a continuous elastic description during the activation of the myocardium, we used an approach similar to the one proposed by Chadwick [4], Ohayon and Chadwick [20], Taber [27]. From its passive zero-stress state P, the free activation of the muscle fibers is modeled by the following two transformations (Fig.2): the first one (from state P to virtual state A_0) changes the material properties without changing the geometry, and the second one (from A_0 to A) contracts the muscle without changing the properties of the material. Thus, the former is not an elastic deformation and is described by the gradient tensor $\mathbf{\Phi}_{PA_0} = \mathbf{I}$ where $\mathbf{I}$ is the identity matrix. In that first transformation, only the strain energy function is modified using an activation function β, which may depend on the cardiac cycle time and some ionic concentration (calcium for instance). The second transformation is an elastic deformation caused only by the active tension delivered by the fibers and takes care of the internal kinematic constraint (Eq.(1)). This last transformation is described by the gradient tensor $\mathbf{F}_{A_0A}$. Thus the transformation from state P to state A is a non elastic transformation ($\mathbf{\Phi}_{PA} = \mathbf{\Phi}_{PA_0}\mathbf{F}_{A_0A}$), but can be treated mathematically as an elastic one because $\mathbf{\Phi}_{PA} = \mathbf{F}_{A_0A}$. Finally, external loads are applied to state A deforming the body through into C (Fig. 3).

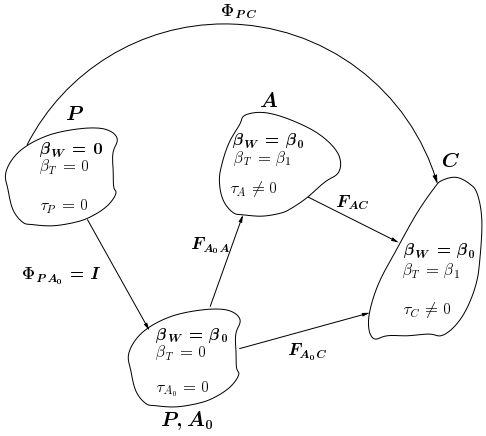

Figure 3: Description of the active rheology approach.

The change of the material properties of the myocardium during the cardiac cycle is described by a parameter-dependent strain-energy function per unit volume of state P noted $W(\mathbf{E}_{PH})$:

$$W(\mathbf{E}_{PH}) = -\frac{1}{2}\, p_H(I_3(\mathbf{E}_{PH}) - 1) + W^*(\mathbf{E}_{PH}) + \delta_{AH}\, W^{pseudo}_{active}(\mathbf{E}_{PH}) \tag{2}$$

with

$$W^*(\mathbf{E}_{PH}) = W_{pas}(\mathbf{E}_{PH}) + \beta\, W^f_{act}(\mathbf{E}_{PH}) \tag{3}$$

where $\mathbf{E}_{PH}$ is the Green's strain tensor at an arbitrary state H calculated from the zero strain state P (the state H could be one of the states A_0, A or C shown in figure 3), p_H is the Lagrangian multiplier resulting of the incompressibility constraint $\det \mathbf{\Phi}_{PH} = 1$ (see [8, 16, 12]), $I_3(\mathbf{E}_{PH})$ is the determinant of the right Cauchy-Green strain tensor $\mathbf{C}_{PH}$ ($\mathbf{C}_{PH} = 2\mathbf{E}_{PH} + \mathbf{I}$), W_{pas} represents the contribution of the surrounding collagen matrix and of the passive fiber components, W^f_{act} arise from the active component of the embedded muscle fibers, and β is an activation parameter equal to zero at end-diastolic state and equal to one at end-systolic state ($0 \leq \beta \leq 1$). The scalar δ_{AH} is equal to one if state H is the state A and zero if the two states H and A are distinct. The term $W^f_{act}(\mathbf{E}_{PH})$ gives the variation of the muscle fibers properties during the cardiac cycle. The pseudo-active strain energy function expressed in the last term of the right hand side of the Eq.(2) is introduced in order to satisfy the kinematic condition (Eq.(1)) and is given by:

$$W^{pseudo}_{active}(\mathbf{E}_{PH}) = -\frac{1}{2} q_H\, h(\mathbf{E}_{PH}) \tag{4}$$

The scalar q_H introduced in Eq.(4) serves as an additional indeterminate Lagrange multiplier which contributes to the pseudo-active stresses at state H in fiber and the cross-fiber directions, and $h(\mathbf{E}_{PH})$ is the function defined in Eq.(1), which may be rewritten as:

$$h(\mathbf{E}_{PH}) = 1 - I_6^{1/2} + (\pi - 2)\,(1 - I_4^{-1/4})\,\frac{a}{D} \tag{5}$$

where I_4 and I_6 are two strain invariants given by $I_4(\mathbf{E}_{PH}) = \mathbf{f}_P \cdot \mathbf{C}_{PH} \cdot \mathbf{f}_P$ and $I_6(\mathbf{E}_{PH}) = \mathbf{f}^{\perp}_P \cdot \mathbf{C}_{PH} \cdot \mathbf{f}^{\perp}_P$ in which the fiber and the perpendicular fiber directions (this last one corresponding to the direction of the collagen struts) are respectively characterized in state P by the unit vectors $\mathbf{f}_P$ and $\mathbf{f}^{\perp}_P$. In an arbitrary deformed state H, the direction of these two unit vectors are noted $\mathbf{f}_H$ and $\mathbf{f}'_H$ and are respectively defined by:

$$\mathbf{f}_H = \frac{\mathbf{\Phi}_{PH} \cdot \mathbf{f}_P}{\parallel \mathbf{\Phi}_{PH} \cdot \mathbf{f}_P \parallel} \quad \text{and} \quad \mathbf{f}'_H = \frac{\mathbf{\Phi}_{PH} \cdot \mathbf{f}^{\perp}_P}{\parallel \mathbf{\Phi}_{PH} \cdot \mathbf{f}^{\perp}_P \parallel} \quad .$$

The tensor $\mathbf{C}_{PH}$ is the right Cauchy-Green strain tensor ($\mathbf{C}_{PH} = 2\mathbf{E}_{PH} + \mathbf{I} = \mathbf{\Phi}^T_{PH}\mathbf{\Phi}_{PH}$). The superscript 'T' is used for the transpose matrix and $\parallel \cdot \parallel$ stands for the euclidian norm. Note that I_4 and I_6 are directly related respectively to the fiber and cross-fiber extension ratios (we have $I_4 = \lambda^2_f$ and $I_6 = \lambda^2_{cf}$). In our notations λ_f is related to the fiber direction $\mathbf{f}_H$ and λ_{cf} to the cross-fiber direction

$\mathbf{f}'_H$ (Figure 2). We treat the myocardium as a homogeneous, incompressible, and hyperelastic material transversely isotropic with respect to the local muscle fiber direction.
In this study, the passive strain-energy function is [15]

$$W_{pas}(\mathbf{E}_{PH}) = C_1^p(e^Q - 1) \tag{6}$$

$$\text{with} \qquad Q = C_2^p(I_1-3)^2 + C_3^p(I_1-3)(I_4-1) + C_4^p(I_4-1)^2 \tag{7}$$

For the active strain-energy we modified the function found by Lin and Yin [15] by substracting the "beating term" C_5^a:

$$W_{act}(E_{PH}) = C_1^a(I_1-3)(I_4-1) + C_2^a(I_1-3)^2 + C_3^a(I_4-1)^2 + C_4^a(I_1-3) \tag{8}$$

where $C_i^p, \quad i = 1, \cdots, 4$ and $C_i^a, \quad i = 1, \cdots 4$ are material constants and I_1 is the first principal strain invariant given by $I_1(\mathbf{E}_{PH}) = tr\,\mathbf{C}_{PH}$.
The beating term is defined as the part of the active strain-energy function responsible for the change of geometry when the muscle is activated and submited to no external loading. To incorporate the beating behavior, the parameter-dependent beating tension $\beta\, T^{(0)}$ was applied in the deformed fiber direction. In our approach, the active loaded state C of the myocardial tissue is obtained in two steps. In the first step and at a given degree of activation β, we derived and quantified the internal pseudo-active stresses by looking the free contraction configuration of the tissue (state A, Figure 3). Then, in a second step we applied the loads on the active myocardial tissue under the internal pseudo-active stresses previously found.

Step 1: determination of the free contraction state A**-** During the cardiac cycle and at a given degree of activation β, the Cauchy stress tensor in state A (noted $\boldsymbol{\tau}_A$) is given by:

$$\boldsymbol{\tau}_A = -p_A\mathbf{I} + \boldsymbol{\Phi}_{PA}\frac{\partial W^*(\mathbf{E}_{PA})}{\partial \mathbf{E}_{PA}}\boldsymbol{\Phi}_{PA}^T + \beta T^{(0)}\mathbf{f}_A \otimes \mathbf{f}_A + \boldsymbol{\tau}_A^{\substack{pseudo\\active}} \tag{9}$$

$$\text{with} \qquad \boldsymbol{\tau}_A^{\substack{pseudo\\active}} = \boldsymbol{\Phi}_{PA}\frac{\partial W_{\substack{pseudo\\active}}(\mathbf{E}_{PA})}{\partial \mathbf{E}_{PA}}\boldsymbol{\Phi}_{PA}^T \tag{10}$$

where the symbol $\otimes$ denotes the tensor product. The postulated mechanical coupling law (Eq.(5)) induces, during the contraction, a pseudo-active stress tensor:

$$\boldsymbol{\tau}_A^{\substack{pseudo\\active}} = T_A^f\,\mathbf{f}_A \otimes \mathbf{f}_A + T_A^{cf}\,\mathbf{f}'_A \otimes \mathbf{f}'_A \tag{11}$$

These two stress tensor components T_A^f and T_A^{cf} are activation-dependent and behave as some internal tensions in the fiber and cross-fiber directions of unit vectors $\mathbf{f}_A$ and $\mathbf{f}'_A$, respectively. These pseudo-active tensions are defined by:

$$T_A^f = 2\,\frac{\partial W_{\substack{pseudo\\active}}}{\partial I_4}\;\|\;\boldsymbol{\Phi}_{PA}\cdot\mathbf{f}_P\;\|^2 \quad ; \quad T_A^{cf} = 2\,\frac{\partial W_{\substack{pseudo\\active}}}{\partial I_6}\;\|\;\boldsymbol{\Phi}_{PA}\cdot\mathbf{f}_P^{\perp}\;\|^2 \tag{12}$$

Step 2: determination of the physiological active loaded state C**-** These previously found internal pseudo-active tensions T_A^f and T_A^{cf} were introduced in the expression of the stress tensor at loaded state C. Therefore, at a given degree of activation β, the Cauchy stress tensor in the physiological state C (noted $\boldsymbol{\tau}_C$) is given by:

$$\boldsymbol{\tau}_C = -p_C\mathbf{I} + \boldsymbol{\Phi}_{PC}\frac{\partial W^*(\mathbf{E}_{PC})}{\partial \mathbf{E}_{PC}}\boldsymbol{\Phi}_{PC}^T + \left(\beta T^{(0)} + T_A^f\right)\mathbf{f}_C \otimes \mathbf{f}_C + T_A^{cf}\,\mathbf{f}'_C \otimes \mathbf{f}'_C \tag{13}$$

The suggested constitutive law for the active myocardium (Eqs.(2)-(13)) allows to simulate the left ventricle behavior during the whole cardiac cycle. Thus, in this law: (i) the anisotropic behavior is incorporated in the expressions of passive, active and pseudo-active strain energy functions by the terms I_4 and I_6, (ii) the kinematic contraction is accounted for by a beating tension $\beta\, T^{(0)}$ in the fiber direction, (iii) the change of properties is expressed by the active strain energy term $\beta\, W_{act}$, and (iv) the coupling effect between the collagen network and the MF is accounted for by the two internal pseudo-active tensions T_A^f and T_A^{cf} in the fiber and cross fiber directions $\mathbf{f}_C$ and $\mathbf{f}'_C$, respectively.

4 Variational formulation and finite element method

The undeformed body state P contains a volume V bounded by a closed surface $\mathcal{A}$, and the arbitrary deformed body state is, as before, noted H. The corresponding position vectors, in cartesian base unit vectors, are $\mathbf{R} = Y^R\mathbf{e}_R$ and $\mathbf{r} = y^r\mathbf{e}_r$, respectively. However, we write the equations with suitable curvilinear systems of world coordinates noted Θ^{A} in the reference configuration (state P) and θ^α in the deformed configuration (state H): see Fig. A in appendix A. In this paper we use the same conventional notations (Table 1 in appendix A) for vectors, tensors and coordinates systems than Costa et al. [6, 7], where:

- Capital letters are used for coordinates and indices of tensor components associated to state P, and lower case letters are related to state H.
- $\mathbf{G}$ and $\mathbf{g}$ are the base vectors in states P and H, respectively, for which parenthetical superscript indicates the associated coordinate system (for example $\mathbf{G}_I^{(x)} = \partial\mathbf{R}/\partial X^I = \mathbf{R}_{,I}^{(x)}$ and $\mathbf{g}_i^{(x)} = \partial\mathbf{r}/\partial x^i = \mathbf{r}_{,i}^{(x)}$).

The Lagrangian formulation of the virtual works principle is given by ([6, 16])

$$\int_V P_H^{IJ}\Phi_{\cdot J}^{\cdot\alpha}\nabla_I(\delta u_\alpha)\,dV = \int_V \rho(b^\alpha - \gamma^\alpha)\delta u_\alpha\,dV + (1-\delta_{AH})\int_{A_2}\mathbf{s}.\boldsymbol{\delta}\mathbf{u}\,dA \tag{14}$$

where P_H^{IJ} are the components of the second Piola-Kirchhoff stress tensor at state H, $\mathbf{P}_H$, referred to the base tensor $\mathbf{G}_I^{(x)}\otimes\mathbf{G}_J^{(x)}$, $\Phi_{\cdot I}^{\cdot\alpha} = \partial\theta^\alpha/\partial X^I$ are the components of the gradient tensor $\boldsymbol{\Phi}_{PH}$ in the base tensor $\mathbf{g}_\alpha^{(\theta)}\otimes\mathbf{G}^{(x)I}$, $\boldsymbol{\delta}\mathbf{u} = \delta u_\alpha\mathbf{g}^{(\theta)\alpha}$ is an arbitrary admissible displacement vector, $\nabla_I(\delta u_\alpha) = \partial\delta u_\alpha/\partial X^I - \mathbf{g}_{\alpha,I}^{(\theta)}\cdot\mathbf{g}^{(\theta)\beta}\delta u_\beta$ are the components of the covariant differentiation vector $\boldsymbol{\delta}\mathbf{u}$ in the base vectors $\mathbf{g}^{(\theta)\alpha}$ (i.e. $\nabla_I(\delta u) = \nabla_I(\delta u_\alpha)\mathbf{g}^{(\theta)\alpha}$). The previous differentiation is done with respect to the locally orthonormal body coordinates (X^I, $I = 1,2,3$) which coincide with the local muscle fiber direction in state P. The material density in the undeformed body state P is ρ, $\mathbf{b} = b^\alpha\mathbf{g}_\alpha^{(\theta)}$ is the body force vector per unit mass, $\boldsymbol{\gamma} = \gamma^\alpha\mathbf{g}_\alpha^{(\theta)}$ is the acceleration vector, $\mathbf{s}$ is the surface traction per unit area of $\mathcal{A}$, and A_2 is the part of $\mathcal{A}$ not subject to displacement boundary conditions.The Lagrangian formulation for incompressibility is given by

$$\int_V \left(\det g_{IJ}^{(x)} - 1\right)\,p^*\,dV = 0 \tag{15}$$

where the metric tensor $g_{IJ}^{(x)}$ is defined in table 1, and p^* is an arbitrary admissible pressure. Lastly the Lagrangian formulation for the additional pseudo-active kinematic constraint is given by

$$\delta_{AH}\int_V h(I_4, I_6)\,q^*\,dV = 0 \tag{16}$$

for all admissible q^*. Eqs.(14)-(15) -(16) represent the variational formulation of a system of nonlinear partial differential equations. For an incompressible medium ($\det\boldsymbol{\Phi}_{PH} = 1$), the relation between the second Piola-Kirchoff stress tensor $\mathbf{P}_H$ and the Cauchy stress tensor $\boldsymbol{\tau}_H$ is ([16])

$$\mathbf{P}_H = \boldsymbol{\Phi}_{PH}^{-1}\,.\,\boldsymbol{\tau}_H\,.\,(\boldsymbol{\Phi}_{PH}^{-1})^T \tag{17}$$

A complete expression of the components of $\mathbf{P}_H$ in both states $H = A$ and $H = C$ are given in appendix B. The surface traction per unit of undeformed area of $\mathcal{A}$, $\mathbf{s} = s^\alpha\mathbf{g}_\alpha^{(\theta)}$, is a known loading boundary which could be written using physical Cauchy stress.

4.1 Finite element approximation

Through this paper, we use a three dimensional finite element with Lagrange trilinear interpolation for the displacements and uniform Lagrangian multipliers to compute an approximate solution of Eqs.(14)-(15)-(16) on a rectangular mesh (see Fig. 4.1), where we neglect the acceleration and body forces ($\mathbf{b} = 0$, $\boldsymbol{\gamma} = 0$). This element is commonly used and is relevant for the finite element approximation of this type of problem where kinematics constraints must be satisfied (for more details see [18, 9, 10, 11, 5, 22]).

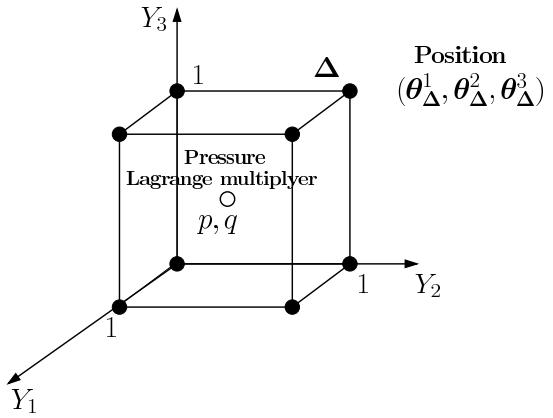

Figure 4: $Q1 - Q0$ element for displacements, pressure and pseudo-active Lagrange multiplyer.

Let (ξ_K) the Lagrangian normalized finite element coordinates (Figure A), the deformed geometric coordinates θ^α in element e are interpolated as

$$\theta^\alpha = \sum_{n(e)=1}^{8} \psi_{n(e)}(\xi_1, \xi_2, \xi_3)\, \theta^\alpha_{n(e)} \tag{18}$$

where $\psi_{n(e)}$ is the base function associated with the local node $n(e)$ and $\theta^\alpha_{n(e)}$ is the α-coordinate of the local node n of element e.

Let $\Omega^{n(e)}_\Delta$ be the connectivity matrix defined by

$$\Omega^{n(e)}_\Delta = \left\{ \begin{array}{ll} 1 & \text{if} \quad \Delta(n(e), e) = \Delta \\ 0 & \text{otherwise} \end{array} \right. \tag{19}$$

The FE approximation of Eqs.(14)-(15)-(16) is

$$\sum_e \sum_{n(e)=1}^{8} \Omega^{n(e)}_\Delta \int_{V_e} P^{IJ}_H\, \Phi^{\cdot\alpha}_J\, \nabla_I(\psi_{n(e)})\, dV \;=\; (1 - \delta_{AH}) \sum_e \sum_{n(e)=1}^{8} \Omega^{n(e)}_\Delta \int_{A_{2_e}} s^\alpha\, \psi_{n(e)}\, dA \tag{20}$$

$$\forall e\,, \int_{V_e} \Big(\det g^{(x)}_{IJ} - 1 \Big)\, dV \;=\; 0 \tag{21}$$

$$\forall e\,, \delta_{AH} \int_{V_e} h(I_4, I_6)\, dV = 0 \tag{22}$$

with $\Delta = 1, \cdots, \Delta_{max}$, $\alpha = 1, 2, 3$, where V_e is the volume of the element e, A_{2_e} is the part of A_e (boundary of the element e) non subject to displacement conditions.

4.2 Finite element solution method

We proceed in two steps. The first one consists in the determination of the pseudo- active stresses T^f_A and T^{cf}_A as functions of the activation parameter $\beta \in [0, 1]$ by looking for the state A ($\delta_{AH} = 1$). We solve the system (20)-(21)-(22) with zero right hand side for (20) (free active contraction) and P^{IJ}_A given by Eq.(26) . The unknowns of this nonlinear system of equations are $(\theta^\alpha_\Delta, p_A(e), q_A(e))$ with $\alpha = 1, 2, 3$, $\Delta = 1, \cdots, \Delta_{max}$ and $e = 1, \ldots, e_{max}$ where e_{max} is the total number of elements involved in the mesh. We derive T^f_A and T^{cf}_A for a given β according to Eq.(12). Then in a next step we can compute any physiological active loaded state C solving the system (20)-(21) with $\delta_{AH} = 0$ and P^{IJ}_C given by Eq.(27). To solve the sytem in both cases we use the Powell method [21] implemented in the package MINPACK [17].

5 Results and discussion

This section is devoted to the numerical simulation of two types of material:

- a thin sample of living myocardium for which a cartesian coordinate is used,
- an active thick-walled cylinder for which cylindrical coordinate is used.

For these two simple configurations the exact displacements are solutions of a nonlinear system and can be computed with a high degree of accuracy. A very good agreement between the exact and the computed solutions of the finite element nonlinear system (20)-(21)-(22) is obtained. More precisely in all the cases the L^2 norm of the error is less than 10^{-09}.

5.1 Case of a thin sample of living myocardium

We simulated the loading of a thin sample of living myocardium ($1.0 \times 1.0 \times 0.1$ cm^3) in which the MF are uniformly oriented in one direction. The coefficients involved in the strain energy-function are those of Lin and Yin [15]: C_1^p=0.292 kPa, C_2^p=0.321, C_3^p=-0.260, C_4^p=0.201, C_1^a=-3.870 kPa, C_2^a=4.830 kPa, C_3^a=2.512 kPa and C_4^a=0.951 kPa. For the beating tension, a good agreement between the previous experimental results and our theoretical solution is obtained for $T^{(0)}$=0.6 kPa. Nevertheless, the control simulation was performed with a/D=0.2 and $T^{(0)}$=35 kPa. This higher value of $T^{(0)}$ is more adapted to the description of the left ventricular performance [19].

Influence of the collagen network on the systolic wall thickening- The free contraction test is performed with no external displacement or force on the boundaries of the sample, but just in activating the tissue. In this simulation we used the following activation function : $\beta(s) = sin^2(\pi s)$. Compare to the case where the kinematic constraint is not taken into account, one can see an increase of the cross-fiber extension ratio which is in the tangential plane of the ventricular wall (Figure 5). At the end-systolic state (i.e. when $\beta = 1$), this ratio goes from the value 1.25 if we neglect the coupling effect, to 1.45 when considering the kinematic constraint induced by the collagen. So, the connective tissue could account for 16 % of normal end-systolic wall thickness. This increase is clearly dependent of the geometrical parameter ratio a/D and the maximal beating tension $T^{(0)}$.

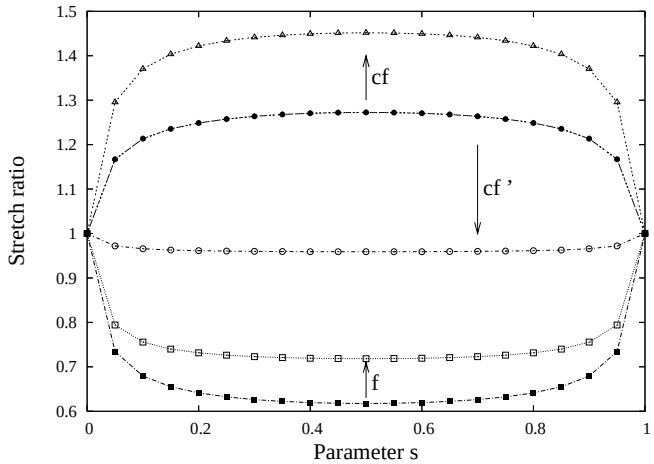

Figure 5: Free contraction test with $\beta(s) = sin^2(\pi s)$: effect of the pseudo-active kinematic constraint. The empty and full symbols indicate that the coupling effect is acting or not, respectively. The fiber and cross-fiber directions are noted (f), (cf) and (cf ') and are defined in figure 2. Arrows show the curve modification when the pseudo-active kinematic constraint behaves.

Influence of the collagen network on the pseudo-active tension- Table 1 shows the effect of the geometrical parameter a/D and the maximal active tension $T^{(0)}$, on the fiber and cross-fiber stresses (noted σ_{11} and σ_{22}, respectively). These effects were given in the case of an equibiaxial extension loading ($\lambda_f = \lambda_{cf} = 1.2$) of an activated sample of myocardium ($\beta = 1$). These two stresses increase with $T^{(0)}$, but are not very sensitive to the geometrical ratio a/D. We can observe also, that by neglecting

the interaction between the collagen network and the MF: (i) the cross-fiber stress is not affected by the amplitude of the beating tension, and (ii) the stress ratio σ_{22}/σ_{11} decreases when $T^{(0)}$ increases. These results mean that the usual strain-energy functions considered for the myocardium are not able to generate any transverse pseudo-active tension. Moreover, the results obtained for the uniaxial tests of an active or a passive sample, with or without the effect of the collagen on the MF, are shown in Figure 6. Because the coupling effect between the collagen and the MF is an active mechanism, the passive stress-strain relations are not affected by the kinematic constraint. The mechanical properties of the active tissue, in the fiber and cross-fiber directions, become comparable when the coupling effect acts.

Table 1: Effect of active tension $T^{(0)}$ and geometrical parameter a/D

a/d \ T_0 (KPa)		5	15	25	35	45
0.10	σ_{22}/σ_{11} (%)	50.92	53.73	57.65	60.25	61.90
	σ_{22} (KPa)	5.94	11.44	17.78	24.32	30.88
0.15	σ_{22}/σ_{11} (%)	51.44	54.56	58.60	61.30	63.01
	σ_{22} (KPa)	5.97	11.48	17.80	24.31	30.84
0.20	σ_{22}/σ_{11} (%)	51.94	55.33	59.47	62.25	64.04
	σ_{22} (KPa)	6.00	11.51	17.79	24.25	30.73
No kinematic constraint	σ_{22}/σ_{11} (%)	36.78	19.88	13.62	10.36	8.36
	σ_{22} (KPa)	4.32	4.32	4.32	4.32	4.32

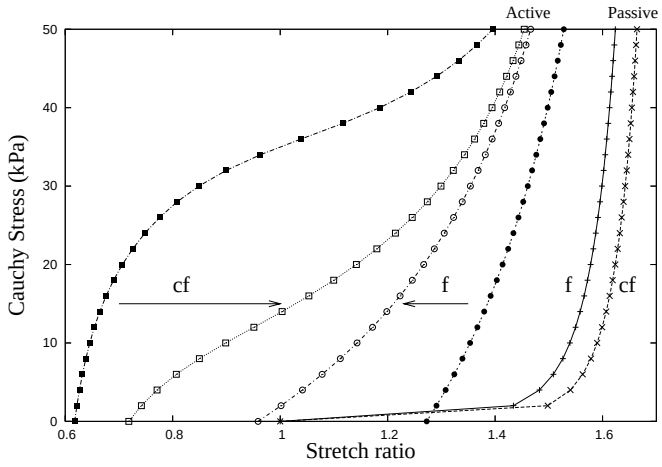

Figure 6: Active and passive uniaxial extension tests: effect of the pseudo-active kinematic constraint. The empty and full symbols indicate that the coupling effect is acting or not, respectively. The fiber and cross-fiber directions noted (f) and (cf) are defined in figure 2. Arrows show the curve modification when the pseudo-active kinematic constraint behaves.

5.2 Case of an active thick-walled cylinder

We simulate the mechanical behaviour of an active artery under physiological blood pressure P_{int}. This artery is modelled by a thick-walled cylinder with internal radius $R_{int} = 2$ mm, external radius $R_{ext} = 3.5$ mm and height $L = 2$ cm. We assume that the medium is made of a hyperelastic anisotropic material with fibers oriented in the circumferential direction. This simulation does not take into account all the complexity of the structure of an artery, so the following results must be viewed as a first approach and we focus on some qualitative aspects, particularly the wall thickening effect.

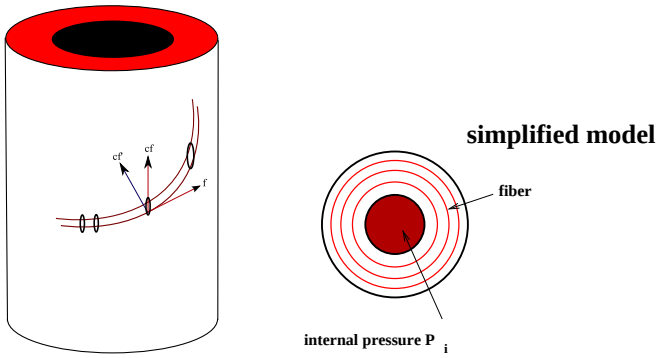

Figure 7: a simplified model for the spatial organization of the collagen fibrils. The fibrils are oriented in the z-direction (cf) and in the right part of the figure we suggest that the fibers are oriented in the circumferential direction

In 1902, Bayliss suggested that the distension of the vessel by blood pressure could act as a mechanical stimulus to the vascular smooth muscle cells, thereby contributing to their tone [1]. However, conclusive experimental support for this concept was available only recently. We now know that the degree of vascular distension appears to be a factor of importance in determining vascular tone. We used the suggested constitutive law to model a hypothetical autoregulation mechanism.
For this simulation, the active fiber tension as well as the rheological change are in phase with the pulsatile pressure, and we use as input data the following functions: $\beta(s) = \sin^2 \pi s$ with $P_{int} = 8 + 10 \sin^2 \pi t$ (Fig. 8). The resulting variations of the thick-walled cylinder radii are presented in Figures 10-11 for this autoregulation law based on fluid pressure. The autoregulation is defined as the relationship between the activation function $\beta(s)$ and the pulsatile blood pressure P_{int}. Very interestingly, the results show that the kinematics of the arterial wall may be more sensitive to the change of mechanical properties than to the blood pressure. In other words, it appears that if there is no kinematic constraint due to the fibrils, the internal and external radii increase when the blood pressure decreases. In fact, during this decrease of pressure, we assume that the material becomes more compliant. Thus, the wall kinematics is mainly driven by the change of rheology. Furthermore, although the pressure and activation are in phase, you can create with this autoregulation law some delay in the kinematic response. Therefore we believe that the pressure-activation interaction is a fundamental mechanism which must be well modeled to describe accurately the behaviour of the arterial wall under physiological or pathological conditions [28, 24].
On the other hand, when the kinematic constraint is activated, we observe that the interior radius still decreases but less than previously, due to the residual constraints T_A^f and T_A^{cf} (see Fig. 10). The more important effect is observed for the exterior radius (Fig. 11), due to a greater residual constraints T_A^f and T_A^{cf} and the absence of exterior stress. The global result is a wall thickening effect and a contraction in the z-direction due to the incompressibility condition (see Fig. 9)

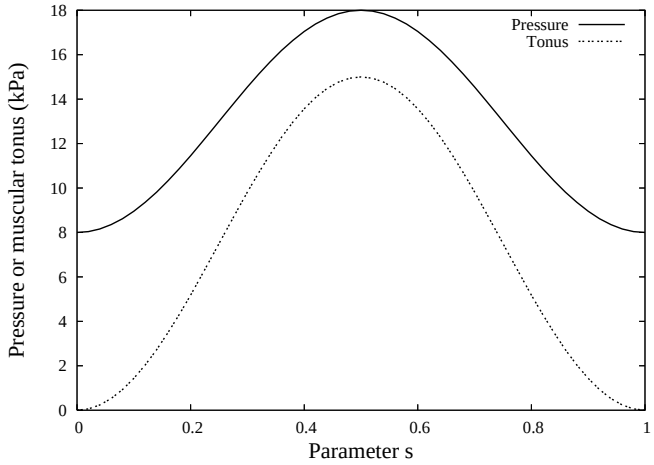

Figure 8: Pressure and tonus as a function of the degree of activation

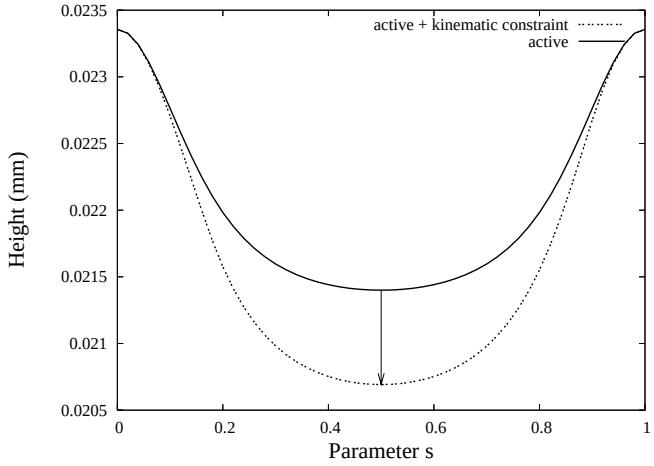

Figure 9: height of the cylinder as a function of the degree of activation

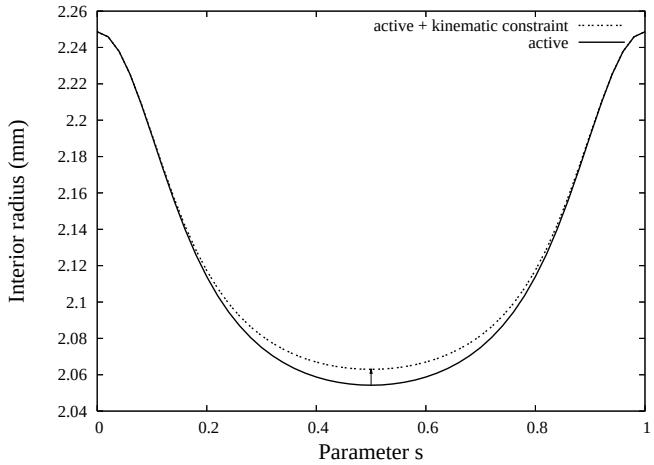

Figure 10: interior radius of the cylinder as a function of the degree of activation

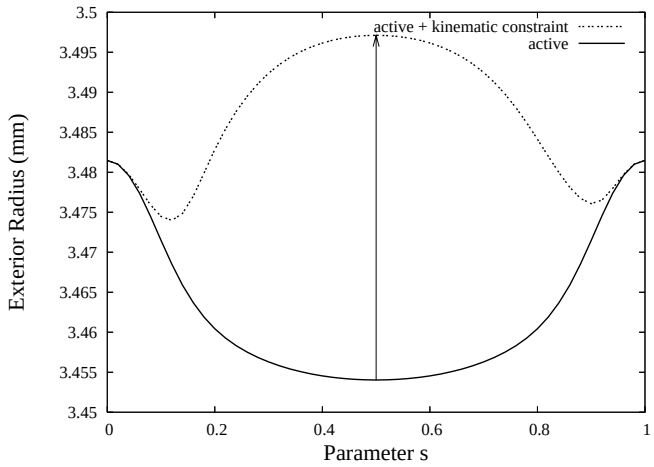

Figure 11: exterior radius of the cylinder as a function of the degree of activation

6 Conclusion

This study shows that the connective tissue skeleton in the normal and pathological left ventricle may have a large influence on the cardiac performance. A new constitutive law has been developed for large deformations of an incompressible hyperelastic, and anisotropic living myocardium. This work is based on the idea that the connective tissue is physically coupled to the muscle fibers which seems reasonable with regard to the available observations. Nevertheless, additional experimental works must be done in order to support this assumption and to study thoroughly the spatial organization of the myocardial collagen fibrils under normal and pathological conditions.

A Coordinate systems

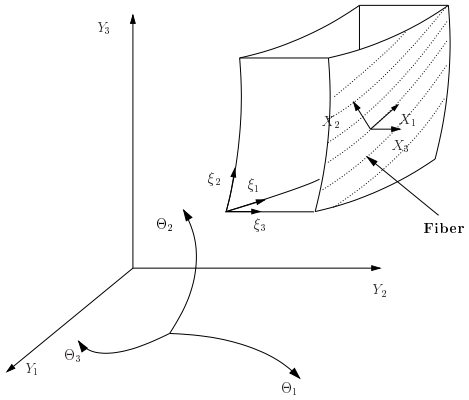

Figure 12: Coordinate systems (adapted from Costa et al. [6]).

Table 2: Notations for the coordinate systems used to formulate the finite element method (adapted from Costa et al. [6]). (I) Rectangular cartesian reference coordinates, (II) Curvilinear world coordinates, (III) Normalized finite element coordinate, (IV) Locally orthonormal body/fiber coordinates (adapted from Costa et al. [6]).

	State	Indices	Coord.	Covariant basis vectors	Contravariant basis vectors	Metric tensors	
(I)	P	R, S	Y^R	$\mathbf{e}_R$	$\mathbf{e}_R$	δ_{RS}	δ^{RS}
	C	r, s	y^r	$\mathbf{e}_r$	$\mathbf{e}_r$	δ_{rs}	δ^{rs}
(II)	P	A, B	Θ^A	$\mathbf{G}^{(\theta)}_A = \dfrac{\partial \mathbf{R}}{\partial \Theta^A}$	$\mathbf{G}^{(\theta)A}$	$G^{(\theta)}_{AB}$	$G^{(\theta)AB}$
	C	α, β	θ^α	$\mathbf{g}^{(\theta)}_\alpha = \dfrac{\partial \mathbf{r}}{\partial \theta^\alpha}$	$\mathbf{g}^{(\theta)\alpha}$	$g^{(\theta)}_{\alpha\beta}$	$g^{(\theta)\alpha\beta}$
(III)	P	K, L	ξ^K	$\mathbf{G}^{(\xi)}_K = \dfrac{\partial \mathbf{R}}{\partial \xi^K}$	$\mathbf{G}^{(\xi)K}$	$G^{(\xi)}_{KL}$	$G^{(\xi)KL}$
	P	I, J	X^I	$\mathbf{G}^{(x)}_I = \dfrac{\partial \mathbf{R}}{\partial X^I}$	$\mathbf{G}^{(x)I}$	$G^{(x)}_{IJ} = \delta_{IJ}$	$G^{(x)IJ} = \delta^{IJ}$
	C			$\mathbf{g}^{(x)}_I = \dfrac{\partial \mathbf{r}}{\partial X^I}$	$\mathbf{g}^{(x)I}$	$g^{(x)}_{IJ}$	$g^{(x)IJ}$

B Second Piola-Kirchoff stress tensor at states A and C

In the case of the free contraction state A, using Eqs.(4)-(13)-(10)-(17), we can write the components P^{IJ}_A of the second Piola-Kirchoff stress tensor $\mathbf{P}_A$ in the state A base tensor $(\mathbf{G}^{(x)}_I \otimes \mathbf{G}^{(x)}_J)_A$ under the form:

$$\begin{aligned} P^{IJ}_A &= -p_A\, g^{(x)IJ} + 2G^{(x)IJ}\, W^*_1 + (2\, W^*_4 - q_A\, h_4)\, f^{(x)I}_P f^{(x)J}_P \\ &\quad + \beta\, T^{(0)} f^{(x)I}_A f^{(x)J}_A - q_A\, h_6\, f^{\perp(x)I}_P f^{\perp(x)J}_P \end{aligned}$$

while in the case of the active loaded state C, using Eq.(9)-(17), the components P^{IJ}_C of $\mathbf{P}_C$ in the state C base tensor $(\mathbf{G}^{(x)}_I \otimes \mathbf{G}^{(x)}_J)_C$ are

$$\begin{aligned} P^{IJ}_C &= -p_C\, g^{(x)IJ} + 2G^{(x)IJ}\, W^*_1 + 2\, W^*_4\, f^{(x)I}_P f^{(x)J}_P \\ &\quad + (\beta\, T^{(0)} + T^f_A)\, f^{(x)I}_C f^{(x)J}_C + T^{cf}_A\, f^{'(x)I}_C f^{'(x)J}_C \end{aligned}$$

$$\text{where} \qquad W^*_i = \frac{\partial W^*}{\partial I_i} = \frac{\partial W_{pas}}{\partial I_i} + \beta\, \frac{\partial W^f_{act}}{\partial I_i} + \delta_{AH}\, \frac{\partial W^{\ pseudo}_{\ active}}{\partial I_i} \quad i = 1,\, 4 \tag{23}$$

$$\text{and} \qquad h_i = \frac{\partial h(I_4, I_6)}{\partial I_i} \quad i = 4,\, 6 \tag{24}$$

$f^{(x)I}_P$, $f^{\perp(x)I}_P$ are respectively the components of the unit vectors $\mathbf{f}_P$, $\mathbf{f}^\perp_P$ in the base $(\mathbf{G}^{(x)}_I,\ I = 1, 2, 3)$ and $f^{(x)I}_H$, $f^{'(x)I}_H$ with $H = A$ or C, are respectively the components of the unit vectors $\mathbf{f}_H$, $\mathbf{f}'_H$ in the base

$(\mathbf{g}_I^{(x)},\ I=1,2,3)$. The metric tensors $G^{(x)IJ}$, $g^{(x)IJ}$ are defined in table 1.
Following the definition of the locally orthonormal body/fiber coordinate system we have $f_P^{(x)I}=\delta^{1I}$ and $f_P^{\perp(x)I}=\delta^{2I}$. On the other hand the vectors $\mathbf{f}_H$ and $\mathbf{f}'_H$ are respectively defined through:

$$\mathbf{f}_H=\frac{\mathbf{\Phi}_{PH}\mathbf{f}_P}{\parallel \mathbf{\Phi}_{PH}\mathbf{f}_P \parallel}=\frac{\mathbf{f}_P^{(x)I}\mathbf{g}_I^{(x)}}{\parallel \mathbf{f}_P^{(x)I}\mathbf{g}_I^{(x)} \parallel} \quad \text{and} \quad \mathbf{f}'_H=\frac{\mathbf{\Phi}_{PH}\mathbf{f}_P^{\perp}}{\parallel \mathbf{\Phi}_{PH}\mathbf{f}_P^{\perp} \parallel}=\frac{\mathbf{f}_P^{\perp(x)I}\mathbf{g}_I^{(x)}}{\parallel \mathbf{f}_P^{\perp(x)I}\mathbf{g}_I^{(x)} \parallel} \tag{25}$$

thus $f_H^{(x)I}=\dfrac{\delta^{1I}}{\parallel \mathbf{g}_1^{(x)} \parallel}$ and $f_H^{'(x)I}=\dfrac{\delta^{2I}}{\parallel \mathbf{g}_2^{(x)} \parallel}$ and we get finaly:

$$\begin{aligned} P_A^{IJ} &= -p_A\, g^{(x)IJ}+2G^{(x)IJ}\,W_1^*+(2\,W_4^*-q_A\,h_4)\,\delta^{1I}\delta^{1J} \\ &\quad +\beta\,T^{(0)}\frac{\delta^{1I}\delta^{1J}}{\parallel \mathbf{g}_1^{(x)} \parallel^2}-q_A\,h_6\,\delta^{2I}\delta^{2J} \end{aligned} \tag{26}$$

and

$$\begin{aligned} P_C^{IJ} &= -p_C\, g^{(x)IJ}+2G^{(x)IJ}\,W_1^*+2\,W_4^*\,\delta^{1I}\delta^{1J} \\ &\quad +(\beta\,T^{(0)}+T_A^f)\,\frac{\delta^{1I}\delta^{1J}}{\parallel \mathbf{g}_1^{(x)} \parallel^2}+T_A^{cf}\,\frac{\delta^{2I}\delta^{2J}}{\parallel \mathbf{g}_2^{(x)} \parallel^2} \end{aligned} \tag{27}$$

References

[1] W.M. Bayliss. *On the local reaction of the arterial wall to changes of internal pressure.* J. Physiol. London, 8:220–231, 1902.

[2] J. B. Caulfield and J. S. Janicki. *Structure and function of myocardial fibrillar collagen.* Technol. Health Care, 5:95–113, 1997.

[3] R. S. Chadwick, A. Tedgui, J.B Michel, J. Ohayon, and B. I Levy. *Phasic regional myocardial inflow and outflow : comparison of theory and experiments.* Am. J. Physiol., 258:H1687–1698, 1990.

[4] R.S. Chadwick. *Mechanics of the left ventricle.* Biophys. J., 39:279–288, 1982.

[5] P. G. Ciarlet. *The finite element method for elliptic problems*, volume 4 of Studies in Mathematics and its Applications. North-Holland, Amsterdam -New York, 1980.

[6] K.D. Costa, P.J. Hunter, J.S. Wayne, L.K. Waldman, J.M. Guccione, and A.D. McCulloch. *A three-dimensional finite element method for large elastic deformations of ventricular myocardium: Part I - Cylindrical and spherical polar coordinates.* ASME J. Biomech. Eng, 118:452–463, 1996.

[7] K.D. Costa, P.J. Hunter, J.S. Wayne, L.K. Waldman, J.M. Guccione, and A.D. McCulloch. *A three-dimensional finite element method for large elastic deformations of ventricular myocardium: Part II - Prolate spheroidal coordinates.* ASME J. Biomech. Eng, 118:464–470, 1996.

[8] Y.C. Fung. *Foundations of solid mechanics.* Prentice-Hall, 1965.

[9] R. Glowinsky and P. Le Tallec. *Numerical solution of problems in incompressible finite elasticity by augmented lagrangian methods: I. Two-dimensional and axisymetric problems.* SIAM J. Appl. Math., 42:400–429, 1984.

[10] R. Glowinsky and P. Le Tallec. *Numerical solution of problems in incompressible finite elasticity by augmented lagrangian methods: II. Three-dimensional problems.* SIAM J. Appl. Math., 42:710–733, 1984.

[11] R. Glowinsky and P. Le Tallec. *Augmented lagrangian and operator-splitting methods in nonlinear mechanics.* SIAM, Philadelphia, PA, 1989.

[12] A.E. Green and W. Zerna. *Theoretical Elasticity*. Dover Publication, 1992.

[13] J.M. Huyghe, D.H. van Campen, T. Arts, and R.M. Heethaar. *A two-phase finite element model of the diastolic left ventricle*. J. Biomech., 24:527–538, 1991.

[14] I.J. LeGrice IJ, Y. Takayama, and J.W.J. Covell. *Transverse shear along myocardial cleavage planes provides a mechanism for normal systolic wall thickening*. Circ. Res., 77:182–193, 1995.

[15] D.H.S. Lin and F.C.P. Yin. *A multiaxial constitutive law for mammalian left ventricular myocardium in steady-state barium contracture or tetanus*. J. Biomech. Eng., 120:504–517, 1998.

[16] L. E. Malvern. *Introduction to the mechanics of a continuous medium*. Prentice-Hall, 1969.

[17] J.J. Morge, B. S. Garbow, and K. E. Hillstrom. *User Guide for MINPACK-1*. Technical Report ANL–80–74, Argonne National Laboratory, March 1980.

[18] J.T. Oden. *Finite elements of nonlinear continua*. McGraw-Hill, New York, 1972.

[19] J. Ohayon, H. Cai, P.S. Jouk, Y. Usson, and A. Azancot. *A model of the structural and functional development of the normal human fetal left ventricle based on a global growth law*. Comp. Meth. Biomech. & Biomed. Engin., 5(2):113–126, 2002.

[20] J. Ohayon and R.S. Chadwick. *Effects of collagen microstructure on the mechanics of the left ventricle*. Biophys. J., 54:1077–1088, 1988.

[21] M.J.D. Powell. *A hybrid method for nonlinear equations*. In P. Rabinowitz, editor, *Numerical methods for nonlinear algebraic equations*, pages 87–114, New York, 1970. Gordon and Breach.

[22] A. Quarteroni and A. Valli. *Numerical approximation of partial differential equations*, volume 23 of Springer Series in Computational Mathematics. Springer Verlag, Berlin, 1994.

[23] M.A. Rossi. *Connective tissue skeleton in the normal left ventricle and in hypertensive left ventricular hypertrophy and chronic chagasis myocarditis*. Med. Sci. Monit., 7(4):820–832, 2001.

[24] G.M. Rubanyi. *Mechanoreception by the vascular wall*. Futura Publishing Company, Inc., 1993.

[25] S.J. Sarnoff, E. Braunwald, G.H. Jr. Welch, R. B. Case, W. N. Stainsby, and R. Macruz. *Hemodynamic determinants of oxygen consumption of the heart with special reference to the tension-time index*. Am. J. Phsysiol., 192:148–156, 1958.

[26] D.D. Streeter. *Gross morphology and fiber geometry of the heart*. In R. M. Berne et al., editor, *Handbook of physiology*, volume 1, pages 61–112, Bethesda MD, 1979. American Physiological Society.

[27] L.A. Taber. *On a nonlinear theory for muscle shells: Part II- Application to the beating left ventricle*. J. Biomech. Eng., 113:63–71, 1991.

[28] P. Teppaz, J. Ohayon, and R. Herbin. *Interaction fluide-structure active: écoulement artériel*. C. R. Acad. Sci. Paris, 324(IIb):37–45, 1997.

[29] T.P. Usyk, J.H Homens J.H., and A.D. McCulloch. *Regional septal dysfunction in a three-dimensional computational model of focal myofiber dissaray*. Am. J. Physiol. Heart Circ. Physiol., 281(2):506–514, 2001.